

Relational Representation Learning Network for Cross-Spectral Image Patch Matching

Chuang Yu^{1,2,3,4}, Yunpeng Liu^{1,2*}, Jinmiao Zhao^{1,2,3,4}, Dou Quan⁵, Zelin Shi^{1,2}

¹Key Laboratory of Opto-Electronic Information Processing, Chinese Academy of Sciences

²Shenyang Institute of Automation, Chinese Academy of Sciences

³Institutes for Robotics and Intelligent Manufacturing, Chinese Academy of Sciences

⁴University of Chinese Academy of Sciences

⁵Xidian University

Abstract—Recently, feature relation learning has drawn widespread attention in cross-spectral image patch matching. However, existing related research focuses on extracting diverse relations between image patch features and ignores sufficient intrinsic feature representations of individual image patches. Therefore, we propose an innovative relational representation learning idea that simultaneously focuses on sufficiently mining the intrinsic features of individual image patches and the relations between image patch features. Based on this, we construct a Relational Representation Learning Network (RRL-Net). Specifically, we innovatively construct an autoencoder to fully characterize the individual intrinsic features, and introduce a feature interaction learning (FIL) module to extract deep-level feature relations. To further fully mine individual intrinsic features, a lightweight multi-dimensional global-to-local attention (MGLA) module is constructed to enhance the global feature extraction of individual image patches and capture local dependencies within global features. By combining the MGLA module, we further explore the feature extraction network and construct an attention-based lightweight feature extraction (ALFE) network. In addition, we propose a multi-loss post-pruning (MLPP) optimization strategy, which greatly promotes network optimization while avoiding increases in parameters and inference time. Extensive experiments demonstrate that our RRL-Net achieves state-of-the-art (SOTA) performance on multiple public datasets.

Index Terms — Cross-spectral image patch matching, Image intrinsic features, Relational representation learning

I. INTRODUCTION

IMAGE patch matching is to determine whether image patches come from the same interest point or have the same identity. It is widely used in image registration [1-3], image retrieval [4, 5], re-identification [6, 7], multi-view stereo reconstruction [8, 9] and other fields. Different from object detection and object segmentation tasks that require the precise location of object boundaries [10-13], image patch matching focuses on measuring the similarity between image patches [14, 15]. Considering that single-spectral images have limitations, cross-spectral image matching can establish the correspondence between different spectral images, providing a basis for making full use of the complementary information [16-20]. Of course, compared with single-spectral image patch matching, cross-spectral image patch matching not only faces illumination changes and geometric changes, but also needs to

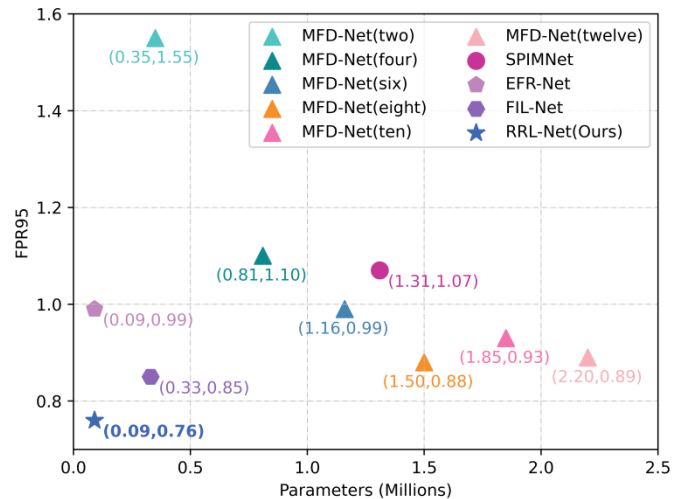


Fig. 1. Performance comparison of multiple excellent cross-spectral image patch matching networks on the VIS-NIR patch dataset. The closer to the origin, the better the network performance. The content in the brackets of MFD-Net denotes the number of network branches. Our RRL-Net achieves SOTA performance. Compared with the lightweight EFR-Net [21], RRL-Net has the same parameters and reduces the FPR95 by **23.2%** (from 0.99 to 0.76). Compared with the latest and most competitive FIL-Net [15], RRL-Net reduces the FPR95 by **10.6%** (from 0.85 to 0.76) and reduces the number of parameters by **72.7%** (from 0.33 to 0.09).

overcome pixel-level nonlinear differences between cross-spectral image patches [15, 21].

Early cross-spectral image patch methods are mainly inspired by research on single-spectral image patches [22, 23] to construct non-deep learning methods [24-28]. However, non-deep learning-based methods have limited feature extraction capabilities. Subsequently, deep learning-based methods have gradually become a trend. Early deep learning-based cross-spectral image patch matching methods use individual image patch features for discrimination [16, 29, 30]. Considering that this task is to measure the similarity between image patches, the relation learning between image patch features is better than the learning of individual image patch features [14, 15, 21]. Therefore, subsequent deep learning-based methods [15, 18-21, 31, 32] focus on extracting diverse relations between image patch features. However, sufficient representation of the individual image patch intrinsic features is the basis for subsequent mining of feature relations. Only focusing on diverse feature relations will limit the improvement of matching performance.

To solve this problem, an innovative relational representation learning idea is proposed for the first time, which simultaneously focuses on fully mining the intrinsic features of individual image patches and the relations between image patch features. This idea breaks the bottleneck of subsequent feature relation extraction caused by insufficient intrinsic feature mining of individual image patches in existing methods and provides a new exploration direction for subsequent research on methods based on feature relation learning. Specifically, we construct an innovative autoencoder. The intrinsic features of individual image patches are fully characterized by using self-supervised learning. At the same time, a feature interaction learning (FIL) module is introduced to interactively learn the intrinsic features of image patches to mine rich and deep-level feature relations.

Considering the small size of image patches and the goal of the matching task being to explore overall similarity rather than strong correspondence between pixels, we consider that in addition to the local features of image patches, global features should be given more attention. Therefore, we propose a multi-dimensional global-to-local attention (MGLA) module, which can extract global features from multiple dimensions and mine local dependencies within global features. The parameters of the MGLA module are negligible. In addition, combined with the MGLA module, we further explore the feature extraction network (encoder), and an attention-based lightweight feature extraction (ALFE) network is constructed, which not only has powerful feature extraction capabilities but also has few parameters.

Considering that reasonably strong supervision can promote matching network optimization, we propose a multi-loss post-pruning (MLPP) optimization strategy, which not only has the advantage of promoting network optimization by adding feature reconstruction branches and multiple metric networks, but also avoids the disadvantages of increasing parameters and reducing inference speed.

In summary, we propose a Relational Representation Learning Network (RRL-Net) to fully characterize the effective feature relations between image patches. From Fig. 1, our RRL-Net has achieved significant performance improvements in both matching results and parameters. In addition, we have also achieved SOTA results on multiple other cross-spectral datasets and conducted detailed ablation experiments to verify the effectiveness of each proposed component. Our contributions can be summarized as follows:

(1) An innovative relational representation learning idea is proposed, which breaks the bottleneck of subsequent feature relation extraction caused by insufficient individual intrinsic feature mining in existing methods.

(2) We construct an autoencoder that uses self-supervised learning to fully characterize the individual intrinsic features. At the same time, we introduce a FIL module to mine deep-level feature relations.

(3) To further fully mine individual intrinsic features, a lightweight MGLA module is proposed and an efficient ALFE network is built based on this module.

(4) A MLPP optimization strategy is proposed that can promote network optimization while avoiding increases in the parameters and inference time.

II. RELATED WORK

In this section, we will briefly review single-spectral image patch matching methods, cross-spectral image patch matching methods, and attention mechanisms.

A. Single-spectral Image Patch Matching

Early single-spectral image patch matching methods are mainly non-deep learning methods, including methods based on image grayscale information [33-36] and methods based on handcrafted feature descriptors [22, 23, 37-42]. However, non-deep learning-based methods do not perform satisfactorily in complex image change scenarios. With the development of artificial intelligence, research on deep learning-based methods has gradually become a trend. Deep learning-based methods can be divided into descriptor learning methods and metric learning methods. The descriptor learning method mainly extracts high-level features (descriptors) of individual image patches and uses feature distance to measure the similarity between descriptors. Existing research on descriptor learning methods has focused mainly on improving loss functions [43-51] and sampling strategies [52-55]. For the research on loss functions, it mainly includes hinge embedding loss [43] and triplet loss [44, 45]. Unlike the hinge embedding loss, which uses absolute distance, the triplet loss uses relative distance. Since triplet loss has better stability, subsequent research has mainly combined triplet loss and studies of its variants [46-51]. For the research on sampling strategies, L2-Net [52] proposes a progressive sampling strategy that can learn a large number of generated negative samples. However, most of the generated samples are simple negative samples, which cannot provide sufficient and effective feedback information during network training. Subsequently, fully mining hard negative samples has been widely studied [53-55]. However, paying too much attention to hard negative samples and ignoring the rich information of simple samples may lead to training instability or even collapse. Different from the descriptor learning method, the metric learning method is an end-to-end deep learning network, which focuses on improving the network structure. MatchNet [56] is one of the earliest metric learning methods for image patch matching. Subsequently, [57] constructs and verifies that the matching performance of the 2-channel network that directly calculates feature similarity in the fused feature space is better than the Siamese network and Pseudo-Siamese network that calculate similarity after acquiring features in a separate feature space. Inspired by this, MRAN [14] achieves excellent matching performance by extracting various feature relations between image patches.

B. Cross-spectral Image Patch Matching

Compared with single-spectral image patch matching, research on cross-spectral image patch matching is relatively late, and its early research is deeply inspired by single-spectral image matching methods. Non-deep learning methods for cross-spectral image patch matching mainly include reducing the impact of gradient direction changes between cross-spectral images [24, 25] and making full use of the strong correlation of edges between cross-spectral images [26-28]. However, these non-deep learning-based methods are difficult to fully extract the discriminative features of cross-spectral image patches.

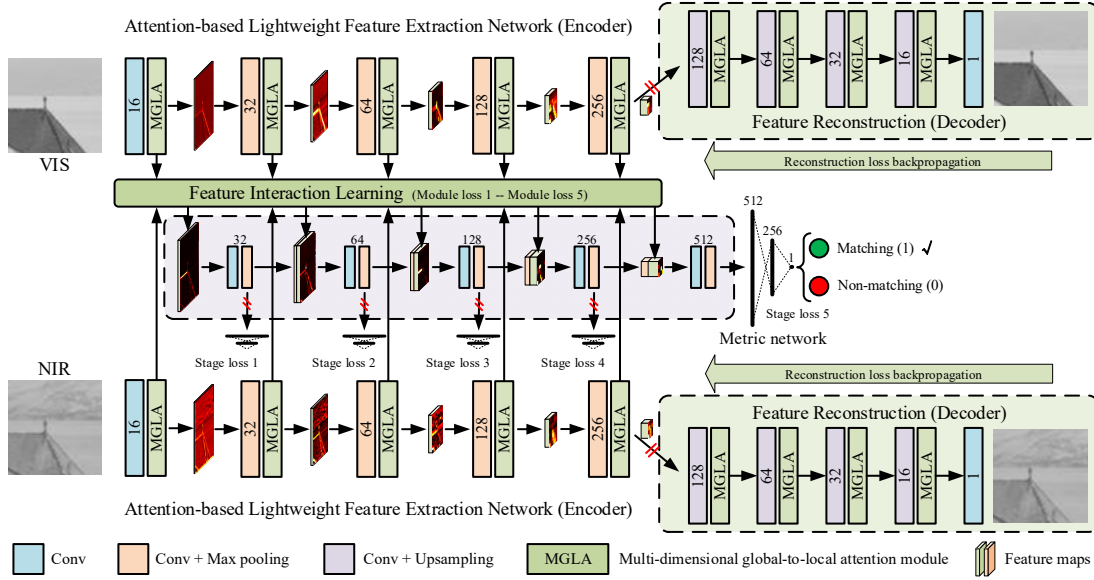


Fig. 2. Network structure of RRL-Net. The red slash denotes the post-pruning operation.

Inspired by [57], [16] proposes Siamese networks, Pseudo-Siamese networks, and 2-channel networks suitable for cross-spectral image patch matching tasks. Compared with non-deep learning methods, all three networks have achieved significant improvement. Subsequently, SCFDM [31] proposes to extract semantically invariant features between cross-spectral image patches in a shared semantic feature space and achieves excellent results, which further reveals that the exploration of feature relations between cross-spectral image patches is superior to the feature extraction of individual image patches. Subsequently, AFD-Net [18, 19] uses feature difference learning to extract differential features between image patches. However, feature difference learning will lose some useful discriminative features while reducing redundant interference features. Therefore, MFD-Net [20] enhances the limited discriminative feature extraction capability of AFD-Net by reasonably constructing a multi-branch network structure. SPIMNet [32] utilizes cross-spectral image patch mutual conversion and feature difference learning to extract effective discriminative features. EFR-Net [21] rationally uses diverse feature relations to effectively mine the differential features and consistent features between cross-spectral image patches with low resource consumption. Although feature relation learning methods such as feature difference learning have achieved excellent results, they can only extract shallow feature relations between image patches. Therefore, [15] proposes a feature interaction learning idea and constructs the FIL-Net, which can extract richer and deeper feature relations. However, the above methods based on feature relation learning focus on extracting diverse relations between image patch features and ignore the full representation of the individual image patch intrinsic features. Sufficient representation of the individual intrinsic features is the basis for subsequent mining of feature relations. Therefore, we explore sufficient representation learning of the individual intrinsic features and the feature relations.

C. Attention Mechanism

Inspired by the human visual system, the attention mechanism focuses on understanding and extracting key useful

information. Generally, neural networks provide implicit attention to extract useful features from data [58]. To enhance the extraction of key features, rationally adding attention mechanisms to neural networks has become a positive trend. A large amount of existing research explores various effective attention structures to improve the performance of deep learning networks on tasks such as machine translation [59], visual recognition [60] and generative models [61].

Vision-based attention mechanisms can be roughly divided into channel attention, spatial attention and self-attention. Channel attention considers the importance of each channel [21, 62-64], such as the SE module [62] and ECA module [63]. Similar to channel attention, spatial attention aims to capture the importance of different regions in the spatial dimension [65-69], such as the CBAM module [66] and SAP module [68]. Self-attention obtains larger receptive fields and contextual information by capturing global information [60, 70-73], such as Non-local block [60] and GC block [72]. Although the above attention mechanisms have achieved great performance improvements in corresponding tasks, there are few existing studies that use attention mechanisms in cross-spectral image patch matching. Therefore, combined with the characteristics of the cross-spectral image patch matching task, we attempt to build an efficient attention mechanism to fully extract the global features of image patches and the local dependencies within the global features.

III. METHOD

A. Overall Architecture

To efficiently extract discriminative features between cross-spectral image patches, we propose a lightweight RRL-Net to fully characterize the feature relations between them. Fig. 2 shows the overall architecture of RRL-Net, which consists of five parts: feature extraction (encoder), feature reconstruction (decoder), feature interaction, feature aggregation and feature metric. For the feature extraction part, we build a lightweight MGLA module that can fully extract

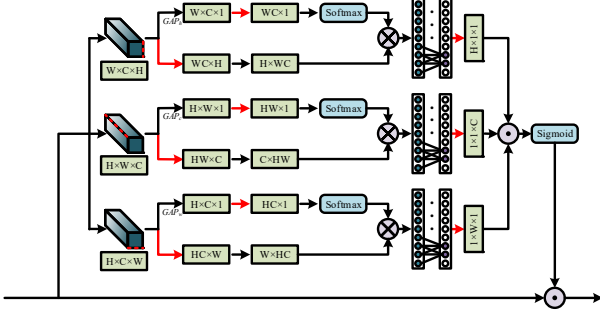


Fig. 3. Structure of the MGLA module. GAP denotes the global average pooling. \otimes denotes the matrix multiplication. \odot denotes the element-wise multiplication. The red arrow denotes the *Reshape* operation.

global features from multiple dimensions and mine local dependencies within global features. In addition, combined with the MGLA module, an efficient ALFE network for cross-spectral image patches is constructed and used. For the feature reconstruction part, we build a feature reconstruction branch, which forms an autoencoder with the ALFE network. The feature reconstruction branch will drive the ALFE network to fully mine individual intrinsic features through self-supervised learning. It is conducive to the subsequent extraction of rich feature relations. Notably, this feature reconstruction branch is pruned before saving the trained model to improve the inference speed. For the feature interaction part, we introduce the FIL module, which was proposed in our previous work [15]. It can effectively extract common features and private features between cross-spectral image patch features. Consistent with [15], we impose reasonable constraints on the common features output by the FIL module to promote the discriminability of the private features to be aggregated. For the feature aggregation part, we aggregate the private features output by the FIL module and learn again to improve feature discriminability. Its detailed structure is shown in the purple area of Fig. 2. For the feature metric part, it contains all metric networks. Specifically, we perform a global average pooling on the feature map to convert it into a one-dimensional (1D) vector and measure the similarity through a 3-layer fully connected network, containing 512, 256 and 1 neurons respectively. Except for the final metric network, which is used to output the similarity, other metric network branches are pruned before the network model is saved.

B. Relational Representation Learning

The goal of cross-spectral image patch matching is to measure the similarity between image patches. The relation learning between image patch features is better than the learning of individual image patch features [14, 15, 21]. Existing methods based on feature relation learning focus on extracting diverse feature relations and ignore the full representation of the individual intrinsic features. However, sufficient representation of the individual intrinsic features is the basis for subsequent mining of feature relations. Therefore, relational representation learning focuses on fully mining two aspects: the intrinsic features of individual image patches and the relations between image patch features.

To fully mine the intrinsic features of individual image patches, on the one hand, we conduct an in-depth exploration of the feature extraction network and propose an ALFE network,

which has efficient image patch feature extraction capabilities and outputs five-stage feature maps. On the other hand, we reconstruct the high-level feature maps generated by the ALFE network using a feature reconstruction network (decoder). By constructing the autoencoder and using self-supervised learning, it is ensured that the ALFE network as the encoder can more fully characterize individual image patch intrinsic features.

To fully explore the relations between image patch features, we introduce the FIL module, which can effectively mine richer and deeper feature relations between cross-spectral image patches. This module fully explores the common and private features between image patches by strengthening the feature interaction and promotes more discriminative private feature output by imposing reasonable constraints on the common features. To fully explore the multi-scale feature relations between image patches, we use five FIL modules on the corresponding feature maps of each stage output by the ALFE network and output five-stage multi-scale private features. At the same time, we use feature aggregation operations to sequentially aggregate multi-stage private features to extract multi-scale discriminative features.

C. MGLA Module

For an image patch with a size of only 64×64 pixels, the effective local features that can be extracted are limited. Convolution is local perception. A feature extraction network constructed by simply stacked convolution will extract a large number of invalid or repeated local features. Although the global features of image patches can be focused on by stacking multiple layers of convolution, it is far from enough. At the same time, unlike tasks such as object segmentation that require precise positioning of object boundaries, matching tasks focus on whether images match. Fully considering the global features of image patches will be more helpful in extracting richer effective features. Therefore, we propose a MGLA module and reasonably embed it into the feature extraction network.

From Fig. 3, the proposed MGLA module performs the same operation from three different dimensions H , W and C . Below, we will take the channel dimension C as an example to illustrate. We first extract the global context through the attention pooling operation and output a 1D global feature vector. This operation does not contain any learning parameters, and is formulated as:

$$G_c^i = DT \left(Re(\hat{F}^i) \right) \otimes Softmax \left(Re(GAP_c(\hat{F}^i)) \right) \quad (1)$$

where GAP_c denotes global average pooling along the channel dimension. Re denotes the *Reshape* operation. DT denotes the dimension transformation.

Then, to further capture the dependencies between channels [60, 70] and consider the impact of SE-Net compressed channels on performance improvement [63], we perform local interactions within global features:

$$GL_c^i = \varphi_c^i(G_c^i) \quad (2)$$

where φ_c^i denotes the 1D convolution operation on channel dimension C in the i -th MGLA module.

The size of the convolution kernel is determined based on the length of the 1D vector, formulated as:

$$k = \left\lceil \frac{\log_2^{len(G_c^i)} + 1}{2} \right\rceil \quad (3)$$

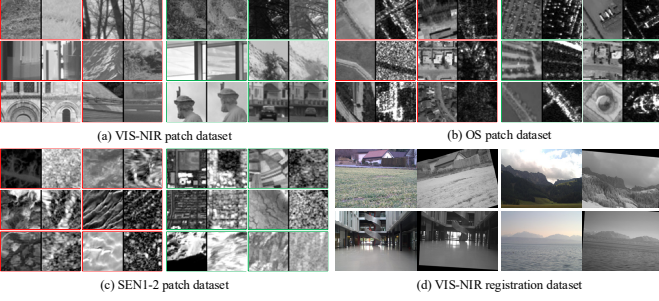


Fig. 4. Partial sample display of multiple datasets.

$$k = \begin{cases} k & k \% 2 = 0 \\ k + 1 & k \% 2 \neq 0 \end{cases} \quad (4)$$

where $\text{len}(G_c^i)$ denotes the 1D global context vector length of the i -th stage. $\lceil \cdot \rceil$ denotes rounding up. k denotes the 1D convolution kernel size. $\%$ denotes the remainder.

Each pixel in the image generally has a stronger correlation with its surrounding pixels. To extract richer global effective features and local dependencies within global features, our operation on the channel dimension is extended to spatial dimensions:

$$F^i = \hat{F}^i \odot \left(\text{Sigmoid} \left(\text{Re} \left(GL_h^i \right) \odot \text{Re} \left(GL_w^i \right) \odot \text{Re} \left(GL_c^i \right) \right) \right) \quad (5)$$

where GL_h^i and GL_w^i denote the outputs of spatial dimensions H and W , respectively.

In addition, combined with the MGLA module, we conduct an in-depth exploration of the feature extraction network for cross-spectral image patches. We find that the MGLA module can promote the reduction of stacked convolutions and cross-layer connections at each stage, thereby turning the constructed ALFE network into a lightweight and effective feature extraction network. Detailed experiments are provided in Section IV-C.

D. MLPP Optimization Strategy

We propose a MLPP optimization strategy that can greatly improve matching performance. The overall loss consists of two parts: reconstruction loss and metric loss. It can be formulated as follows:

$$L_{all} = L_m + \alpha \cdot \sum_{j=1}^2 L_r^j \quad (6)$$

where L_{all} , L_m , and L_r^j denote the total loss, metric loss, and reconstruction loss, respectively. α is set to 1.

To fully mine the intrinsic features of individual image patches, we constrain the reconstructed image by a combination of perceptual loss [72] and MSE loss. The reconstruction loss is formulated as:

$$L_r^j = \sqrt{\left(\varphi_p(P_r^j) - \varphi_p(P^j) \right)^2} + \beta \left(\sqrt{\left(P_r^j - P^j \right)^2} \right) \quad (7)$$

where P_r^j and P^j denote the reconstructed image and original image, respectively. φ_p denotes a VGG19 network [73] pretrained on ImageNet [74]. β is set to 0.1.

To fully explore the relations between image patch features, we use multiple metric networks to impose strong constraints on the extracted relation features. On the one hand, we use a

metric network in the FIL module to constrain the extracted common features, which is called module loss. On the other hand, we use a metric network on the aggregated private features output at each stage, which is called stage loss. The metric loss is formulated as:

$$L_m(\hat{y}^i, \hat{y}^j, y) = \sum_{i=a}^5 L_{module}(\hat{y}^i, y) + \sum_{j=b}^5 L_{stage}(\hat{y}^j, y) \quad (8)$$

$$L(\hat{y}, y) = -[y \log(\hat{y}) + (1 - y) \log(1 - \hat{y})] \quad (9)$$

where L_{module} and L_{stage} denote module loss and stage loss, respectively. \hat{y}^i and \hat{y}^j are the actual outputs of the FIL modules and aggregated features through the metric network. y denotes the true label. We call the metric network used to output the final similarity the master metric network. Other metric networks are called sub-metric networks. Considering that excessive constraints on low-level feature maps will cause them to focus too much on semantic features and neglect to extract detailed features that should be provided to the main network, we appropriately reduce the strong constraints on low-level feature maps. The experiments in Section IV-C verify that both a and b should be set to 3.

If the multi-loss strategy is used directly, it will bloat the final model and affect the inference speed. Therefore, we propose a post-pruning strategy. Specifically, before saving the generated model, we prune all branches that do not interfere with the normal output during the inference phase. By using post-pruning, the parameters of the final saved model will be greatly reduced, and the inference speed will be greatly improved. A detailed experimental verification can be found in Section IV-C.

IV. EXPERIMENT

A. Dataset

From Fig. 4, we experiment on four different cross-spectral datasets, in which the cross-spectral image patch size is 64×64 pixels. The details are as follows:

1) *VIS-NIR patch dataset* [16]. It is a visible spectrum (VIS) and near-infrared (NIR) image patch matching dataset based on the VIS-NIR scene dataset [75]. Specifically, the dataset contains more than 1.6 million pairs of cross-spectral image patches with equal positive and negative samples, divided into 9 subsets, namely Country, Field, Forest, Indoor, Mountain, Oldbuilding, Street, Urban, and Water. For the construction of this dataset, VIS image patches cropped based on SIFT keypoints as the center are first acquired. Secondly, half of the VIS image patches and NIR image patches whose keypoint coordinates are consistent form matching samples. Finally, the other half of the VIS image patches and random NIR image patches form non-matching samples. Consistent with [14-16, 18-21, 29-32], only the ‘‘Country’’ subset is used for training, and the other eight subsets are used for testing.

2) *OS patch dataset* [21]. It is a VIS and SAR image patch matching dataset based on the OS dataset [76]. Each image patch is cropped at the center of the keypoints obtained by the SIFT method. Pairs of cross-spectral image patches with the same keypoints are identified as matching samples. Pairs of cross-spectral image patches with different keypoints are

TABLE I
THE IMPACT OF EACH COMPONENT ON MATCHING PERFORMANCE ON THE VIS-NIR PATCH DATASET.

Methods	Variants			FPR95 ↓
	MGLA	FIL	MLPP	
Our-w/o MGLA	✗	✓	✓	1.14 (-33.3%)
Our-w/o FIL	✓	✗	✓	1.02 (-25.5%)
Our-w/o MLPP	✓	✓	✗	1.01 (-24.8%)
RRL-Net (Ours)	✓	✓	✓	0.76

TABLE II
COMPARISON OF VARIOUS ATTENTION MODULES ON THE VIS-NIR PATCH DATASET. R DENOTES THE COMPRESSION RATIO.

Network	Attention modules	FPR95 ↓	Parameters ↓
RRL-Net (w/o MGLA)	-	1.14 (-33.3%)	9,403,905 (+120)
	SE (r = 4) ^[62]	0.93 (-18.3%)	9,492,441 (-0.9%)
	SE (r = 8) ^[62]	0.98 (-22.4%)	9,448,669 (-0.5%)
	SE (r = 16) ^[62]	1.07 (-29.0%)	9,426,783 (-0.2%)
	ECA ^[63]	0.83 (-8.4%)	9,403,953 (+72)
	ELA ^[21]	0.81 (-6.2%)	9,404,025
	CBAM (r = 4) ^[66]	0.97 (-21.6%)	9,493,421 (-0.9%)
	SNL ^[70]	0.94 (-19.1%)	9,580,491 (-1.8%)
	GC (r = 4) ^[70]	0.90 (-15.6%)	9,494,435 (-1.0%)
	MGLA (Ours)	0.76	9,404,025

TABLE III
PERFORMANCE OF THE SINGLE-DIMENSIONAL GLOBAL-TO-LOCAL ATTENTION MODULE ON THE VIS-NIR PATCH DATASET. HGLA, WGLA, AND CGLA DENOTE DIMENSIONS H , W , AND C GLOBAL-TO-LOCAL ATTENTION.

Settings	Attention Module			FPR95 ↓	Parameters ↓
	H	W	C		
Ours-w/o MGLA	✗	✗	✗	1.14 (-33.3%)	9,403,905 (+120)
Ours-w/ HGLA	✓	✗	✗	1.08 (-29.6%)	9,403,941 (+84)
Ours-w/ WGLA	✗	✓	✗	1.05 (-27.6%)	9,403,941 (+84)
Ours-w/ CGLA	✗	✗	✓	0.79 (-3.8%)	9,403,953 (+72)
Ours-w/ MGLA	✓	✓	✓	0.76	9,404,025

TABLE IV
STRUCTURAL EXPLORATION AND PERFORMANCE VERIFICATION OF THE ALFE NETWORK ON THE VIS-NIR PATCH DATASET. CL: CONVOLUTIONAL LAYERS BEFORE EACH MGLA MODULE, CC: CROSS-LAYER CONNECTION.

Methods	CL			CC	FPR95 ↓	Parameters ↓
	1	2	3			
Variant 1	✗	✗	✓	✓	0.83 (-8.4%)	12,648,441 (-25.7%)
Variant 2	✗	✗	✓	✗	0.91 (-16.5%)	12,556,601 (-25.1%)
Variant 3	✗	✓	✗	✓	0.80 (-5.0%)	11,072,153 (-15.1%)
Variant 4	✗	✓	✗	✗	0.84 (-9.5%)	10,980,313 (-14.4%)
Variant 5	✓	✗	✗	✓	0.82 (-7.3%)	9,495,865 (-1.0%)
ALFE (Ours)	✓	✗	✗	✗	0.76	9,404,025

identified as non-matching samples. The number of generated non-matching samples is the same as the number of matching samples. The dataset contains a total of 123,676 samples, of which the training set and the test set contain 98,940 and 24,736 samples respectively. From Fig. 4, compared with the VIS-NIR patch dataset, the VIS-SAR image patch pairs in the OS patch dataset have more obvious nonlinear differences.

3) *SEN1-2 patch dataset* [15]. It is a VIS and SAR image patch matching dataset based on the SEN1-2 dataset [77]. The construction process of this dataset is consistent with the OS patch dataset. This dataset has more samples, containing a total of 800,000 samples, of which the training set and the test set contain 600,000 and 200,000 respectively. From Fig. 4, compared to the OS patch dataset, the scenes in the SEN1-2 patch dataset have less semantic feature information.

4) *VIS-NIR registration dataset*. This registration dataset is a VIS and NIR registration dataset that we construct based on the VIS-NIR scene dataset [75]. It has 160 test sample pairs, which come from the first 20 pairs of each subset. The image pair to be registered is generated by performing an affine transformation including rotation, translation and scaling on the NIR images in the original registered image pair. Consistent with the experiments on the VIS-NIR patch dataset, the experiments are trained on the “Country” subset and tested on the other eight subsets. The dataset we made is available online¹.

B. Experimental Settings

1) *Training details*. The epochs, learning rate, and batch size are set to 40, $2e-4$, and 64, respectively. The GPU is RTX 2080Ti 11G. To avoid the network from falling into overfitting, data augmentation operations such as flipping, rotation, and contrast enhancement are used to generate lots of images and improve model generalization.

2) *Evaluation Metrics*. For image patch matching, the false positive rate at 95% recall (FPR95) [14-16, 18-21, 29-32] and area under the curve (AUC) are used. For cross-spectral image registration, the root mean square error (RMSE) and image registration rate I_{rr} are used [2, 3, 15]. An image after affine transformation with a RMSE less than 5 is called a registered image. In the results presented, bold denotes the optimal results and underline denotes the suboptimal results.

C. Ablation Study

To better verify the robustness and effectiveness of RRL-Net, extensive ablation experiments on the VIS-NIR patch dataset are performed to explore the performance of each component.

1) *Break-down Ablation*. We first explore the impact of each component on performance. From Table I, the MGLA module, FIL module and MLPP optimization strategy can reduce the FPR95 by 33.3%, 25.5% and 24.8%, respectively. These results verify the significant effectiveness of each component.

2) *Attention Scheme Comparison*. For the cross-spectral image patch matching task, it is difficult to fully extract effective features by simply focusing on local features. Therefore, we propose a lightweight MGLA module to extract global features in multiple dimensions and strengthen the local feature interactions within global features. We compare our MGLA module with various attention modules on the VIS-NIR patch dataset. From Table II, firstly, adding an attention module can improve the matching results, and our MGLA module with negligible parameters achieves SOTA results. Secondly, from the results of the SE modules with different compression rates, excessive compression of the channel dimension has a negative impact, and the impact becomes more serious with the increase of compression rate. At the same time, combining the results of

¹ <https://github.com/YuChuang1205/VIS-NIR-registration-dataset>

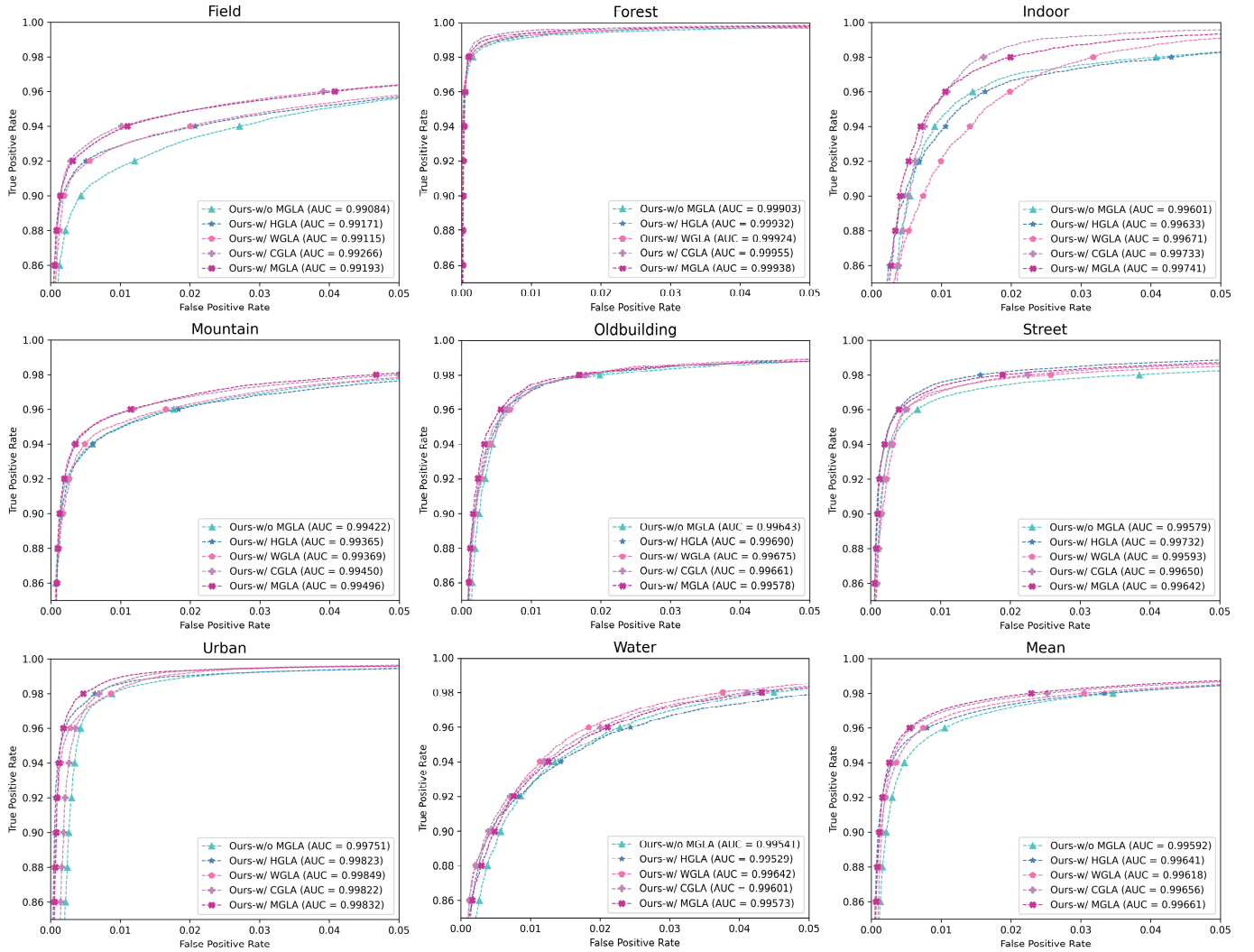


Fig.5. Ablation experiments of the MGLA module on the VIS-NIR patch dataset. The receiver operating characteristic (ROC) curves without using the MGLA module are mostly at the lowest, and those with using the MGLA module are mostly at the highest. From the “Mean” subgraph, compared with not using the MGLA module, the AUC is significantly improved whether using a single-dimensional global-to-local module (HGLA, WGLA, CGLA) or a multi-dimensional global-to-local module (MGLA). In addition, using the final MGLA module has the best AUC.

ECA, ELA and MGLA modules, it can be seen that not using dimensionality reduction but strengthening local interactions within global features will significantly help improve the performance of cross-spectral image patch matching. Finally, from the SE and CBAM modules, simply adding a spatial attention branch to focus on local spatial features will not improve the matching results, but will worsen them. At the same time, combining the results of the SNL, GC and MGLA modules, using attention pooling operations to pay more full attention to global features will significantly help improve the matching results. To sum up, for the cross-spectral image patch matching task, on the one hand, we should pay more attention to the global features of individual image patches to fully exploit the discriminative and effective features. On the other hand, we should strengthen the local interactions within the global features to effectively obtain the local dependencies.

To further explore the performance of the MGLA module, we split the MGLA module into a spatial dimension H global-to-local attention (HGLA) module, a spatial dimension W global-to-local attention (WGLA) module and a channel dimension C global-to-local attention (CGLA) module. From

Table III and Fig. 5, firstly, compared with not using the MGLA module, the results are significantly improved whether using a single-dimensional global-to-local module (HGLA, WGLA, CGLA) or a multi-dimensional global-to-local module (MGLA). This verifies the effectiveness of the global-to-local attention idea. Secondly, the effect of adding the CGLA module is significantly better than that of HGLA and WGLA. This shows that compared with paying attention to other dimensions, fully considering the global context of the image patch and strengthening the local interaction between the global features of the channel dimension can achieve a more significant improvement in matching performance. In addition, compared with the CGLA module, the MGLA module can achieve better matching results with a negligible increase in parameters, which can more comprehensively promote effective feature extraction of image patches.

3) *ALFE network.* Combined with the proposed MGLA module, we conduct an in-depth exploration of the feature extraction network. We explore the number of convolutional layers (before each MGLA module) and cross-layer connections at each stage. [15] achieves the optimal matching

TABLE V

ABLATION EXPERIMENTS EXPLORE THE RATIONALITY OF THE MLPP OPTIMIZATION STRATEGY COMPOSITION ON THE VIS-NIR PATCH DATASET. SMN: SUB-METRIC NETWORK, RB: RECONSTRUCTION BRANCHES, RB LOSS: RECONSTRUCTION BRANCH LOSS, ML: MSE LOSS, PL: PERCEPTUAL LOSS, PP: POST-PRUNING. .

Methods	SMN	RB	RB Loss ML	PL	PP	FPR95 ↓	Parameters ↓	Inference time (s) ↓
Ours-w/o MLPP	✗	✗	✗	✗	✗	1.01 (-24.8%)	9,404,025	0.40×10^{-3}
Variant 1	✗	✓	✓	✓	✗	0.95 (-20.0%)	10,190,175 (-7.7%)	0.51×10^{-3} (-21.6%)
Variant 2	✓	✗	✗	✗	✗	0.83 (-8.4%)	12,043,262 (-21.9%)	0.44×10^{-3} (-9.1%)
Variant 3	✓	✓	✗	✓	✗	0.79 (-3.8%)	12,829,276 (-26.7%)	0.54×10^{-3} (-25.9%)
Variant 4	✓	✓	✓	✗	✗	0.79 (-3.8%)	12,829,276 (-26.7%)	0.54×10^{-3} (-25.9%)
Variant 5	✓	✓	✓	✓	✗	0.76	12,829,276 (-26.7%)	0.54×10^{-3} (-25.9%)
Ours-w/ MLPP	✓	✓	✓	✓	✓	0.76	9,404,025	0.40×10^{-3}

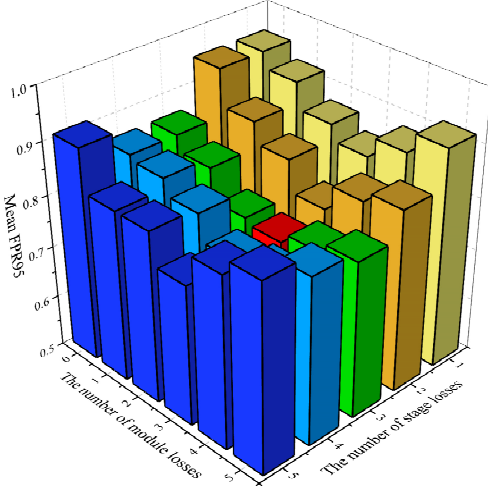


Fig. 6. The results of different combinations of stage loss and module loss on the VIS-NIR patch dataset. Losses are added from higher to lower levels. Red denotes the lowest value of 0.76.

result by using 3 convolutional layers and applying cross-layer connections. However, from Table IV, when using our MGLA module, the optimal number of convolutional layers is 1 and no cross-layer connections are used. At the same time, Compared with Variant 1-Variant 5, the FPR95 and parameters of the ALFE network are reduced by 5.0%-16.5% and 1.0%-25.7%. This shows that the addition of lightweight MGLA modules can reduce the use of network layers and cross-layer connections, and improve the network's ability to extract effective features of image patches.

4) *MLPP optimization strategy.* To effectively verify the performance of our proposed MLPP strategy, we perform many experiments, as shown in Table V. Compared with not using the MLPP strategy, the reasonable addition of sub-metric networks and reconstruction branches will improve the matching results. At the same time, the improvement is more obvious when they are used superimposed, which can reduce the FPR95 by 24.8%. Of course, it will bring about an increase in network parameters and inference time. To solve this problem, we use post-pruning. Compared with simply using the multi-loss strategy, the MLPP optimization strategy has the same matching effect improvement, and its network parameters and single sample inference time are reduced by 26.7% and 25.9%, respectively. It is worth mentioning that compared with only adding sub-metric networks (“Variant 2”), which has

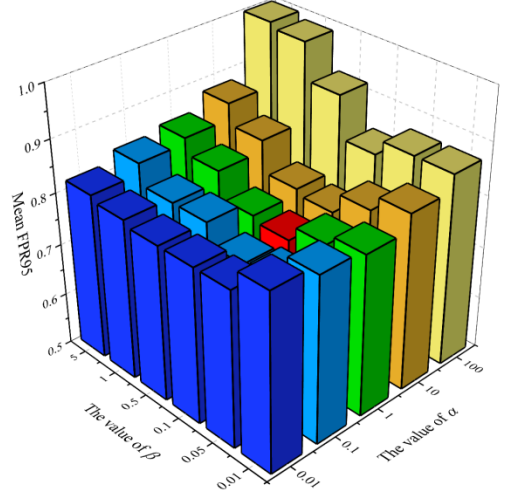


Fig. 7. The results of different combinations of α and β in overall loss on the VIS-NIR patch dataset. The best matching result is achieved when $\alpha = 1$ and $\beta = 0.1$. Red denotes the lowest value of 0.76.

achieved an excellent result of 0.83 in FPR95, adding additional reconstruction branches (“Variant 5”) will reduce FPR95 by 8.4% (from 0.83 to 0.76). This proves that fully mining individual intrinsic features will help break the bottleneck of existing feature relation extraction, thereby achieving a significant improvement in matching performance.

Excessive constraints on the low-level features of the main network will cause it to focus on semantic feature extraction for sub-network discrimination and ignore the extraction of texture detail information for main network discrimination. Therefore, we conduct a detailed exploration of the position of the sub-metric branch to determine the reasonable combination of module losses and stage losses. From Fig. 6, when the added module loss and stage loss are both 3, RRL-Net has the lowest FPR95, which verifies that the reasonable addition of multiple sub-metric branches can effectively improve network performance.

In addition, we conduct experiments to explore the values of α and β , and the experimental results are shown in Fig. 7. First of all, when the value of α is within 0.1-10 and the value of β is within 0.05-0.5, RRL-Net has good matching results. It shows that RRL-Net has a certain degree of stability. At the same time, when α is 1 and β is 0.1, the network has the optimal matching result. In addition, when α is less than 1 or β is less than 0.1 and they become smaller and smaller, FPR95 shows an upward

TABLE VI
COMPARISON OF FPR95 AMONG RRL-NET AND NINETEEN STATE-OF-THE-ART METHODS ON THE VIS-NIR PATCH DATASET.

Models	Field	Forest	Indoor	Mountain	Oldbuilding	Street	Urban	Water	Mean
Traditional methods									
SIFT ^{[22][IJCV 04']}	39.44	11.39	10.13	28.63	19.69	31.14	10.85	40.33	23.95
GISIFT ^{[24][ICIP 11']}	34.75	16.63	10.63	19.52	12.54	21.80	7.21	25.78	18.60
LGHD ^{[28][ICIP 15']}	16.52	3.78	7.91	10.66	7.91	6.55	7.21	12.76	9.16
Descriptor learning									
PN-Net ^{[45][arXiv 16']}	20.09	3.27	6.36	11.53	5.19	5.62	3.31	10.72	8.26
Q-Net ^{[30][Sensors 17']}	17.01	2.70	6.16	9.61	4.61	3.99	2.83	8.44	6.91
L2-Net ^{[52][CVPR 17']}	13.67	2.48	4.63	8.87	4.12	5.58	1.54	6.55	5.93
HardNet ^{[53][NeurIPS 17']}	5.61	0.15	1.50	3.14	1.10	1.93	0.69	2.29	2.05
SOSNet ^{[50][CVPR 19']}	5.94	0.13	1.53	2.45	0.99	2.04	0.78	1.90	1.97
HyNet ^{[51][NeurIPS 20']}	4.50	0.07	1.09	1.80	0.83	0.52	0.53	1.91	1.41
Metric learning									
Siamese ^{[16][CVPRW 16']}	15.79	10.76	11.60	11.15	5.27	7.51	4.60	10.21	9.61
Pseudo-Siamese ^{[16][CVPRW 16']}	17.01	9.82	11.17	11.86	6.75	8.25	5.65	12.04	10.31
2-channel ^{[16][CVPRW 16']}	9.96	0.12	4.40	8.89	2.30	2.18	1.58	6.40	4.47
SCFDM ^{[31][ACCV 18']}	7.91	0.87	3.93	5.07	2.27	2.22	0.85	4.75	3.48
MR_3A ^{[14][TIP 21']}	4.21	0.11	1.12	0.87	0.67	0.56	0.43	1.90	1.23
AFD-Net ^{[18, 19][ICCV'19, TNNLS'21]}	3.47	0.08	1.48	<u>0.68</u>	0.71	0.42	0.29	<u>1.48</u>	1.08
SPIMNet ^{[32][Inf. Fusion'23]}	<u>2.28</u>	0.09	1.62	0.88	0.69	0.29	0.42	2.26	1.07
EFR-Net ^{[21][TGRS'23]}	2.84	0.07	1.09	0.79	0.61	0.50	0.34	1.65	0.99
MFD-Net ^{[20][TGRS'22]}	2.59	0.02	1.24	0.95	<u>0.48</u>	0.24	<u>0.12</u>	1.44	0.88
FIL-Net ^{[15][TIP'23]}	2.61	<u>0.04</u>	<u>0.98</u>	0.73	0.49	0.34	0.10	1.49	<u>0.85</u>
RRL-Net (Ours)	2.16	<u>0.04</u>	0.86	0.59	0.41	<u>0.26</u>	0.14	1.65	0.76

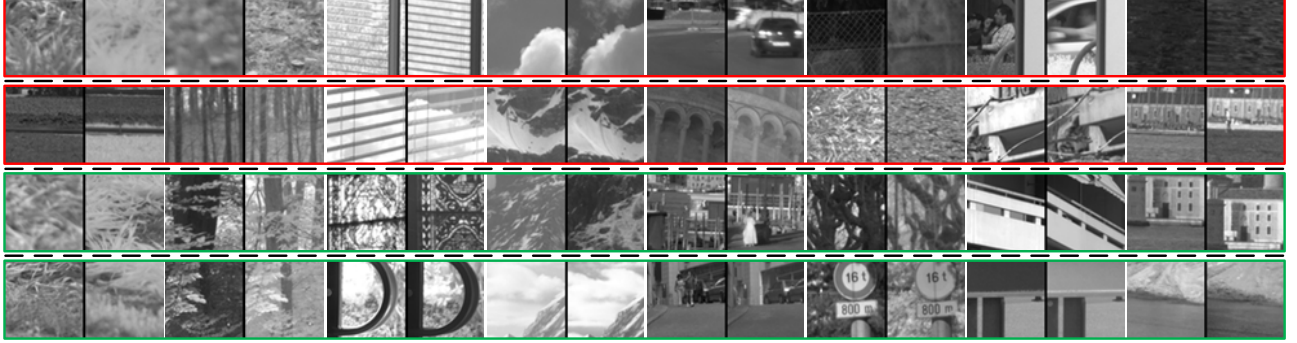


Fig. 8. Partial matching results of RRL-Net on the VIS-NIR patch dataset. From top to bottom, the four lines of samples are misjudged as non-matching, misjudged as matching, correctly judged as non-matching, and correctly judged as matching.

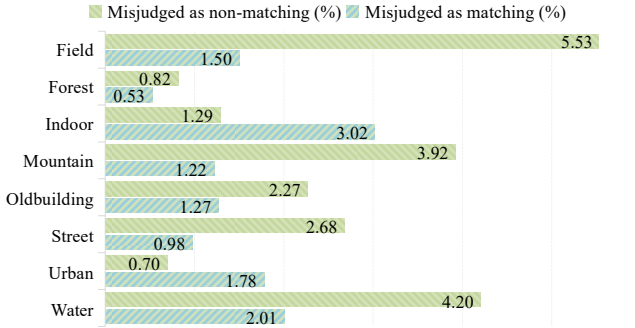


Fig. 9. The misjudgment percentages of RRL-Net on eight subsets.

trend. This is because the constraint of the reconstruction branch will be weakened, resulting in insufficient intrinsic feature mining. When α is greater than 1 or β is greater than 0.1 and they become larger and larger, FPR95 also shows an upward trend and the trend is more obvious. The reason is that overemphasis on intrinsic feature mining and gradual neglect of

subsequent feature relation mining will lead to insufficient discriminative feature extraction, resulting in a significant decrease in the matching effect.

D. Comparison with State-of-the-Art Methods

1) *VIS-NIR image patch matching.* We conduct experiments with 19 state-of-the-art methods on the VIS-NIR patch dataset. From Table VI, on the one hand, it can be found from the individual results of the eight subsets that the proposed RRL-Net achieved optimal results on four subsets, and the results of the remaining four subsets are not much different from the optimal results. On the other hand, from the mean results of eight subsets, RRL-Net achieves state-of-the-art result. Compared with HyNet, the descriptor learning method with the best results, our RRL-Net reduces the mean FPR95 by 46.1% (from 1.41 to 0.76). At the same time, compared with the recent metric learning methods SPIMNet, EFR-Net, MFD-Net and FIL-Net, RRL-Net reduced mean FPR95 by 29.0% (from 1.07 to 0.76), 23.2% (from 0.99 to 0.76), 13.6% (from 0.88 to 0.76) and 10.6% (from 0.85 to 0.76). Notably, compared to MFD-Net in 2022, FIL-Net, which has the best results in 2023,

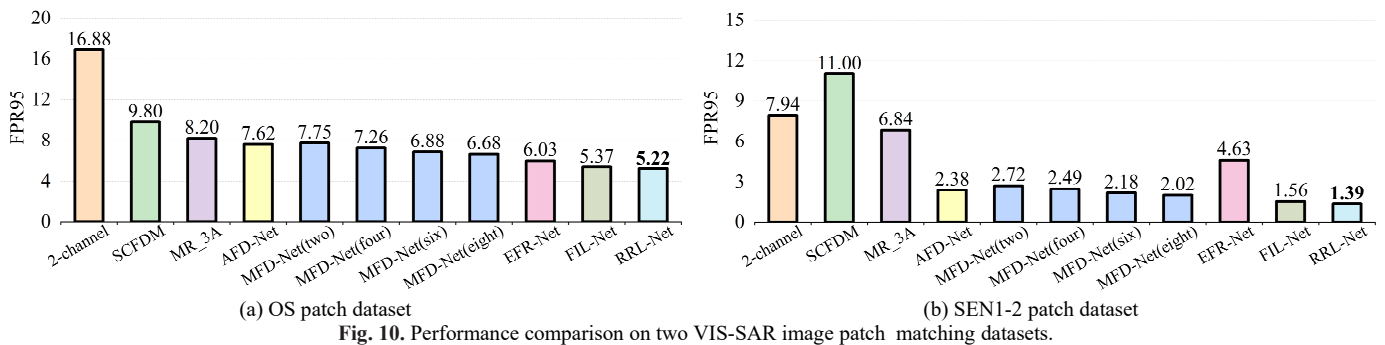


Fig. 10. Performance comparison on two VIS-SAR image patch matching datasets.

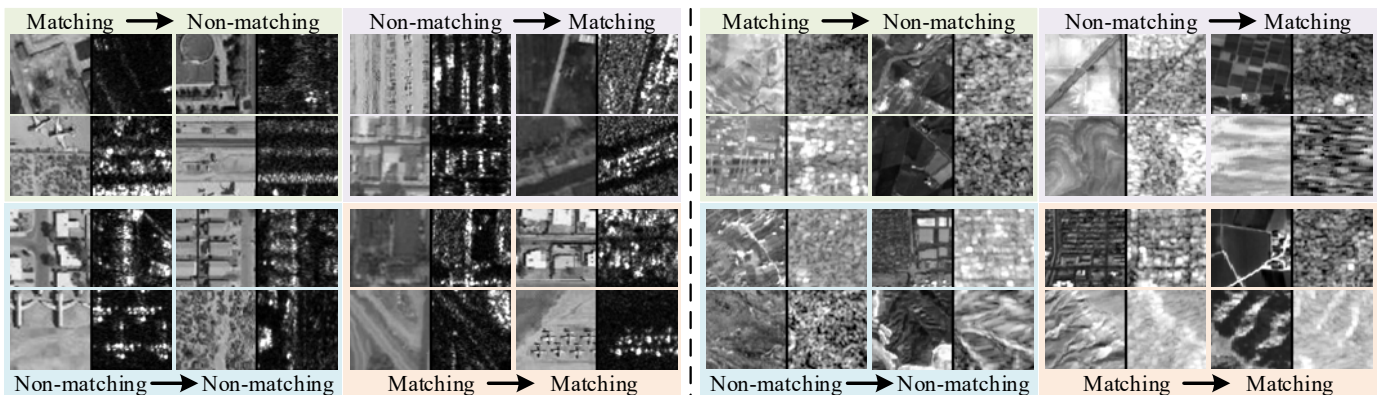


Fig. 11. Partial results of RRL-Net on two VIS-SAR image patch matching datasets. The left and right of the dotted line are the OS patch dataset and the SEN1-2 patch dataset respectively. The left and right sides of the arrow denote the true labels and predicted results.

only decreases by 3.4% (from 0.88 to 0.85). In addition, according to the statistics, the parameters of RRL-Net only account for 27.3% of FIL-Net, and the inference speed of RRL-Net is 1.78 times that of FIL-Net.

To qualitatively analyze the matching effect of RRL-Net in the VIS-NIR scene, Fig. 8 shows some matching results on the VIS-NIR patch dataset. From the samples misjudged as non-matching, most individual samples in pairs have unclear features. At the same time, due to the movement of objects, there are samples that are marked as matching but visually non-matching. From the samples misjudged as matching, most samples have obviously similar semantic features. From the samples that are correctly judged as non-matching, RRL-Net can correctly distinguish non-matching samples with partially similar semantic features. From the samples that are correctly judged as matching, there are obvious nonlinear differences between cross-spectral image patches. This proves that RRL-Net is robust for VIS-NIR scenarios.

To further quantitatively analyze the misjudgment of matching samples and non-matching samples by RRL-Net on the VIS-NIR patch dataset, we present the misjudgment percentage of eight subsets, as shown in Fig. 9. On the whole, the percentage of misjudged as non-matching is significantly greater than the percentage of misjudged as matching. The reason is that the experiment is trained on “Country” and tested on the other eight subsets. Therefore, the matching network can only approximately learn the domain information in the VIS-NIR scenario. There are still different nonlinear differences in the other subsets. On the other hand, it is due to the spatiotemporal difference of collected images. Some moving objects or shooting position deviations will cause the

samples that are finally marked as matching to appear visually non-matching. From the results of each subset, the percentage of samples in “Field”, “Mountain” and “Water” that are misjudged as non-matching is significantly larger. On the one hand, it is due to the influence of the environment. For example, wind has serious spatiotemporal effects on the targets (grass, clouds, water waves) in the corresponding scene. On the other hand, this is due to the influence of the imaging conditions. The scenes in the three subsets are more likely to be too bright or too dark, resulting in a scarcity of single image features in the image patch pairs. This leads to significant nonlinear differences between image patches.

2) *VIS-SAR image patch matching*. We compare our method with 7 state-of-the-art methods on the OS patch dataset and SEN1-2 patch dataset. From Fig. 10(a), our RRL-Net achieves SOTA results on the OS patch dataset. Compared with the methods AFD-Net, MFD-Net(eight), EFR-Net and FIL-Net, RRL-Net reduced FPR95 by 31.5% (from 7.62 to 5.22), 21.9% (from 6.68 to 5.22), 13.4% (from 6.03 to 5.22) and 2.8% (from 5.37 to 5.22), respectively. This shows that our RRL-Net also has good robustness for VIS-SAR cross-spectral image patch matching scenarios. From Fig. 10(b), First, compared to MatchNet, Siamese and Pseudo-Siamese, the other image patch matching methods have achieved significantly better matching results. This shows that learning the feature relations between image patches for the image patch matching task can extract richer discriminative features, especially for image pairs with large nonlinear differences. Secondly, the results of EFR-Net are significantly worse than AFD-Net, MFD-Net, FIL-Net and RRL-Net. This is because EFR-Net only uses high-level feature maps for feature relation learning, while AFD-Net, MFD-Net,

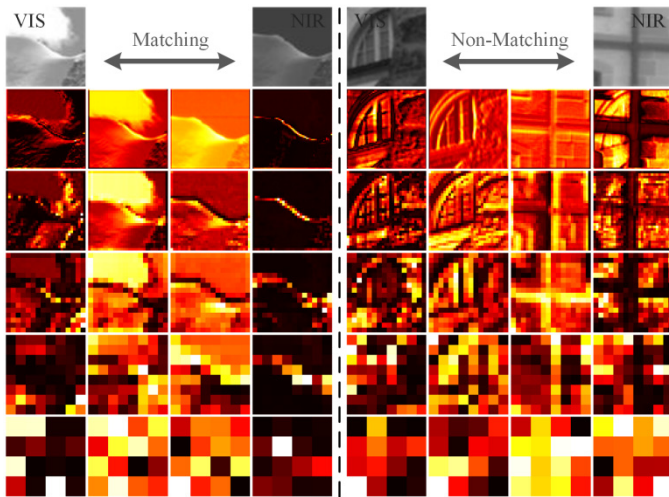


Fig. 12. Visualization of the output feature maps of matching and non-matching VIS-NIR samples after passing through the MGLA modules and the FIL modules. For each pair of samples, the middle two columns denote the output of the MGLA module at each stage, and the left and right columns denote the private feature maps output by the FIL module at each stage. From top to bottom, they denote the stages from shallow to deep.

TABLE VII
REGISTRATION RESULTS OF VARIOUS IMAGE PATCH MATCHING METHODS ON THE VIS-NIR REGISTRATION DATASET.

Methods	RMSE distribution			$I_{rr} \uparrow$	mRMSE \downarrow
	$< 1 \uparrow$	$1 \sim 5$	$> 5 \downarrow$		
SCFDM [31]	121	29	10	93.8%	8.48
AFD-Net [18, 19]	121	29	10	93.8%	9.30
MR_3A [14]	118	31	11	93.1%	10.43
MFD-Net [20]	<u>125</u>	30	5	96.9%	5.57
EFR-Net [21]	124	30	<u>6</u>	<u>96.3%</u>	<u>4.95</u>
FIL-Net [15]	115	38	7	95.6%	5.27
RRL-Net (Ours)	127	27	<u>6</u>	<u>96.3%</u>	4.62

FIL-Net and RRL-Net adopt a multi-stage feature map aggregation structure. For image patch pairs with large nonlinear differences, extracting multi-stage feature maps can significantly improve the extraction of discriminative features. The results of MR_3A, which also uses only high-level feature maps, also illustrate the above point. At the same time, combined with the results on the OS patch dataset, the FPR95 of EFR-Net and MR_3A are not much different between the two datasets, while the FPR95 of AFD-Net, MFD-Net, FIL-Net and RRL-Net are significantly different between the two datasets. On the one hand, it is because the multi-stage feature map aggregation structure requires more samples for network optimization, and the number of samples in the SEN1-2 patch dataset is more than 6 times that of the OS patch dataset. On the other hand, compared to the SEN1-2 patch dataset, the samples in the OS patch dataset have more obvious semantic features, such as houses, airplanes, EFR-Net and MR_3A focus more on high-level semantic features. Finally, our RRL-Net achieves state-of-the-art result on the SEN1-2 patch dataset. Compared with the image patch matching methods AFD-Net, MFD-Net(eight), EFR-Net and FIL-Net, RRL-Net reduces the FPR95 by 41.6% (from 2.38 to 1.39), 31.2% (from 2.02 to 1.39), 70.0% (from 4.63 to 1.39) and 10.9% (from 1.56 to 1.39).

To qualitatively analyze the matching effect of RRL-Net in the VIS-SAR scene, we display some matching results on the OS patch dataset and SEN1-2 patch dataset as shown in Fig. 11. From the samples misjudged as non-matching, there is a common problem of feature scarcity in SAR images. For texture or semantic features in VIS images, there are almost no obvious corresponding features in SAR images. From the samples misjudged as matching, There are large area similar semantic features in VIS and SAR images. From the samples that are correctly judged, RRL-Net can also correctly identify non-matching samples with partially similar semantic features and matching samples with pixel-level nonlinear differences. This proves that RRL-Net has excellent robustness for VIS-SAR image patch matching scenarios.

E. Visualization of feature maps

To further qualitatively analyze the performance of the MGLA module (ALFE Network) and FIL module in RRL-Net, we visualize the feature maps output by the corresponding modules for matching samples and non-matching samples as shown in Fig. 12. On the one hand, regardless of matching samples or non-matching samples, the feature map output by the MGLA module can well characterize the image features and the overall brightness is high. This shows that the ALFE network built based on the MGLA can effectively fully characterize the intrinsic features of image patches. On the other hand, the private feature maps of matching samples are significantly darker than the feature maps output by the MGLA module and the private feature maps of non-matching samples. This verifies that the FIL module can effectively mine the deep-level relations between image patch features, thereby better measuring the similarity between image patches.

F. Application

To further verify the robustness and generalization ability of RRL-Net, we apply our RRL-Net to the cross-spectral image registration task. Consistent with the setting of [15], we first use the SIFT algorithm to extract 1000 keypoints in each image. Secondly, the image patches cropped around the keypoints are combined and input into the RRL-Net to measure the similarity. Then, a nearest neighbor search and threshold filtering are used to find the correspondence between the cross-spectral image patches. Finally, RANSAC [78] is used to eliminate erroneous matches, thereby calculating the registration parameters and achieving registration. From Table VII, although our RRL-Net achieves suboptimal results in registration rate, compared with the optimal registration rate, RRL-Net is only 0.6% different from it. It is worth mentioning that the parameters of RRL-Net only account for 6% of MFD-Net. At the same time, our RRL-Net achieves the best results on mRMSE and is less than 5. The above shows that our RRL-Net has excellent robustness in cross-spectral image registration. In addition, RRL-Net has the most registered samples with RMSE less than 1. This shows that RRL-Net has a more refined registration effect. We also display some registration results on the VIS-NIR registration dataset. From the checkerboard images in Fig. 13, the VIS images after affine transformation almost completely overlap with the NIR images, which proves that RRL-Net has excellent registration results when applied to cross-spectral image registration.

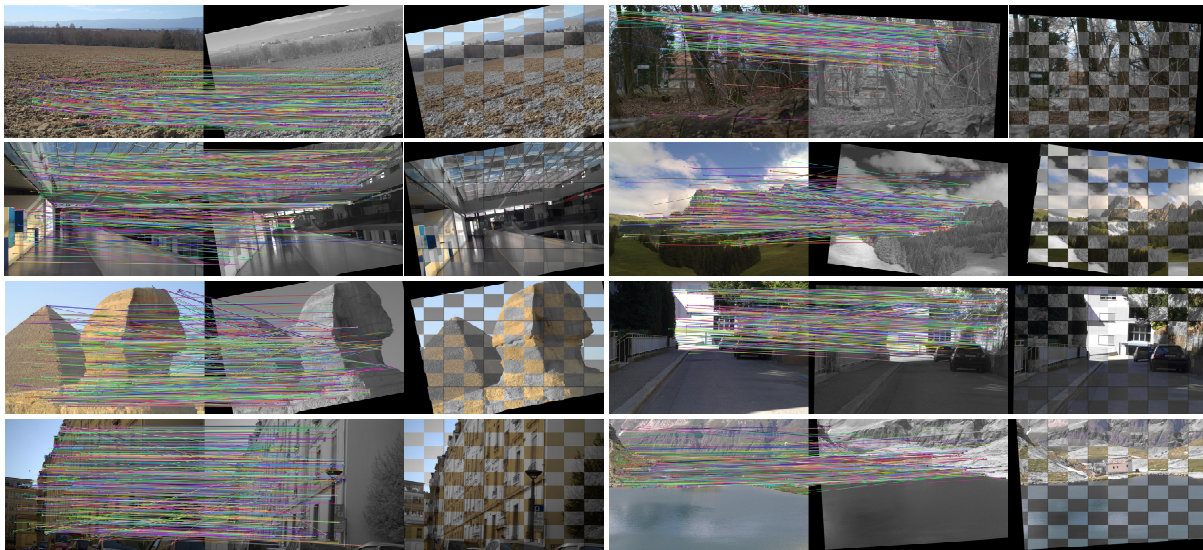


Fig. 13. Partial registration results of RRL-Net on the VIS-NIR registration dataset.

V. CONCLUSION

In this work, we innovatively construct a lightweight RRL-Net, which breaks the bottleneck of subsequent feature relation extraction caused by insufficient intrinsic feature mining of individual image patches in existing methods. To solve the insufficient extraction of individual image patch intrinsic features, on the one hand, we propose a MGLA module and construct an ALFE network. On the other hand, we construct a feature reconstruction branch, which together with the ALFE network forms an autoencoder. For the relations between image patch features, we introduce a FIL module to fully mine the rich and deep-level feature relations. In addition, we construct a MLPP optimization strategy to promote network optimization. The comparison results show that RRL-Net achieves SOTA performance on multiple datasets.

REFERENCES

- [1] S. Wang *et al.*, "A deep learning framework for remote sensing image registration," *ISPRS-J. Photogramm. Remote Sens.*, vol. 145, pp. 148-164, 2018.
- [2] D. Quan *et al.*, "Self-Distillation Feature Learning Network for Optical and SAR Image Registration," *IEEE Trans. Geosci. Remote Sensing*, vol. 60, pp. 1-18, 2022.
- [3] D. Quan *et al.*, "Deep Feature Correlation Learning for Multi-Modal Remote Sensing Image Registration," *IEEE Trans. Geosci. Remote Sensing*, vol. 60, pp. 1-16, 2022.
- [4] Q. Yang, H. Yu, A. Wu, and W. Zheng, "Patch-Based Discriminative Feature Learning for Unsupervised Person Re-Identification," in *Proc. IEEE Conf. Comput. Vis. Pattern Recognit. (CVPR)*, 2019, pp. 3628-3637.
- [5] Y. Chen, L. Wan, Z. Li, Q. Jing, and Z. Sun, "Neural Feature Search for RGB-Infrared Person Re-Identification," in *Proc. IEEE Conf. Comput. Vis. Pattern Recognit. (CVPR)*, 2021, pp. 587-597.
- [6] Y. Shi and H. Li, "Beyond Cross-view Image Retrieval: Highly Accurate Vehicle Localization Using Satellite Image," in *Proc. IEEE Conf. Comput. Vis. Pattern Recognit. (CVPR)*, 2022, pp. 16989-16999.
- [7] F. Lin *et al.*, "Zero-Shot Everything Sketch-Based Image Retrieval, and in Explainable Style," in *Proc. IEEE Conf. Comput. Vis. Pattern Recognit. (CVPR)*, 2023, pp. 23349-23358.
- [8] S. M. Seitz *et al.*, "A Comparison and Evaluation of Multi-View Stereo Reconstruction Algorithms," in *Proc. IEEE Conf. Comput. Vis. Pattern Recognit. (CVPR)*, 2006, pp. 519-528.
- [9] K. Luo, T. Guan, L. Ju, H. Huang, and Y. Luo, "P-MVSNet: Learning Patch-Wise Matching Confidence Aggregation for Multi-View Stereo," in *Proc. IEEE Int. Conf. Comput. Vis. (ICCV)*, 2019, pp. 10451-10460.
- [10] C. Yu *et al.*, "Pay Attention to Local Contrast Learning Networks for Infrared Small Target Detection," *IEEE Geosci. Remote Sens. Lett.*, vol. 19, pp. 1-5, 2022.
- [11] M. He *et al.*, "Cross Domain Object Detection by Target-Perceived Dual Branch Distillation," in *Proc. IEEE Conf. Comput. Vis. Pattern Recognit. (CVPR)*, 2022, pp. 9560-9570.
- [12] Z. Zhou *et al.*, "Generalizable Cross-modality Medical Image Segmentation via Style Augmentation and Dual Normalization," in *Proc. IEEE Conf. Comput. Vis. Pattern Recognit. (CVPR)*, 2022, pp. 20824-20833.
- [13] C. Yu *et al.*, "Precise and Fast Segmentation of Offshore Farms in High-Resolution SAR Images Based on Model Fusion and Half-Precision Parallel Inference," *IEEE J. Sel. Top. Appl. Earth Observ. Remote Sens.*, vol. 15, pp. 4861-4872, 2022.
- [14] D. Quan *et al.*, "Multi-Relation Attention Network for Image Patch Matching," *IEEE Trans. Image Process.*, vol. 30, pp. 7127-7142, 2021.
- [15] C. Yu, Y. Liu, J. Zhao, S. Wu, and Z. Hu, "Feature Interaction Learning Network for Cross-Spectral Image Patch Matching," *IEEE Trans. Image Process.*, vol. 32, pp. 5564-5579, 2023.
- [16] C. A. Aguilera *et al.*, "Learning Cross-Spectral Similarity Measures with Deep Convolutional Neural Networks," in *Proc. IEEE Conf. Comput. Vis. Pattern Recognit. Workshops (CVPRW)*, 2016, pp. 267-275.
- [17] N. Ofir *et al.*, "Deep multi-spectral registration using invariant descriptor learning," in *Proc. IEEE Int. Conf. Image Process. (ICIP)*, 2018, pp. 1238-1242.
- [18] D. Quan *et al.*, "AFD-Net: Aggregated feature difference learning for cross-spectral image patch matching," in *Proc. IEEE Int. Conf. Comput. Vis. (ICCV)*, 2019, pp. 3017-3026.
- [19] D. Quan *et al.*, "Element-Wise Feature Relation Learning Network for Cross-Spectral Image Patch Matching," *IEEE Trans. Neural Netw. Learn. Syst.*, vol. 33, no. 8, pp. 3372-3386, 2021.
- [20] C. Yu *et al.*, "Multibranch Feature Difference Learning Network for Cross-Spectral Image Patch Matching," *IEEE Trans. Geosci. Remote Sensing*, vol. 60, pp. 1-15, 2022.
- [21] C. Yu, J. Zhao, Y. Liu, S. Wu, and C. Li, "Efficient Feature Relation Learning Network for Cross-Spectral Image Patch Matching," *IEEE Trans. Geosci. Remote Sensing*, vol. 61, pp. 1-17, 2023.
- [22] D. G. Lowe, "Distinctive image features from scale-invariant keypoints," *Int. J. Comput. Vis.*, vol. 60, no. 2, pp. 91-110, 2004.
- [23] N. Dalal and B. Triggs, "Histograms of oriented gradients for human detection," in *Proc. IEEE Conf. Comput. Vis. Pattern Recognit. (CVPR)*, 2005, pp. 886-893.
- [24] D. Firminichy, M. Brown, and S. Süsstrunk, "Multispectral interest points for RGB-NIR image registration," in *Proc. IEEE Int. Conf. Image Process. (ICIP)*, 2011, pp. 181-184.
- [25] P. pinggera, T. Breckon, and H. Bischof, "On cross-spectral stereo matching using dense gradient features," in *Proc. Brit. Mach. Vis. Conf.*

- (BMVC), 2012.
- [26] C. Aguilera *et al.*, “Multispectral image feature points,” *Sensors*, vol. 12, no. 9, pp. 12661-12672, 2012.
- [27] T. Mouats, N. Aouf, A. D. Sappa, C. Aguilera, and R. Toledo. “Multispectral stereo odometry,” *IEEE Trans. Intell. Transp. Syst.*, vol.16, no.3, pp. 1210-1224, 2015.
- [28] C. A. Aguilera, A. D. Sappa, and R. Toledo, “LGHD: A feature descriptor for matching across non-linear intensity variations,” In *Proc. IEEE Int. Conf. Image Process. (ICIP)*, 2015, pp. 178-181.
- [29] S. En, A. Lechervy, and F. Jurie, “TS-NET: Combining modality specific and common features for multimodal patch matching,” In *Proc. IEEE Int. Conf. Image Process. (ICIP)*, 2018, pp. 3024-3028.
- [30] C. A. Aguilera, A. D. Sappa, C. Aguilera, and R. Toledo, “Cross-Spectral Local Descriptors via Quadruplet Network,” *Sensors*, vol.17, no. 4, 2017.
- [31] D. Quan, S. Fang, X. Liang, S. Wang, and L. Jiao, “Cross-spectral image patch matching by learning features of the spatially connected patches in a shared space,” In *Proc. Asian Conf. Comput. Vis. (ACCV)*, 2018, pages 115-130.
- [32] Y. Ko, Y. Jang, V. Q. Dinh, H. Jeon, and M. Jeon, “Spectral-invariant matching network,” *Inf. Fusion*, vol. 91, pp. 623-632, 2023.
- [33] D. I. Barnea and H. F. Silverman, “A class of algorithms for fast digital image registration,” *IEEE Trans. Comput.*, vol. 21, no. 2, pp. 179-186, 1972.
- [34] A. Rosenfeld and G. J. Vanderbrug, “Coarse-fine template matching,” *IEEE Transactions on Systems, Man, and Cybernetics*, vol. 7, no. 2, pp. 104-107, 1977.
- [35] G. J. Vanderbrug and A. Rosenfeld, “Two-stage template matching,” *IEEE Trans. Comput.*, vol. 26, no. 4, pp. 384-393, 1977.
- [36] P. Viola and W. M. Wells, “Alignment by maximization of mutual information,” In *Proc. IEEE Int. Conf. Comput. Vis. (ICCV)*, 1995, pp. 16-23.
- [37] Y. Ke and R. Sukthankar, “PCA-SIFT: A more distinctive representation for local image descriptors,” In *Proc. IEEE Conf. Comput. Vis. Pattern Recognit. (CVPR)*, 2004.
- [38] H. Bay, A. Ess, T. Tuytelaars, and L. V. Gool, “Speeded-up robust features (SURF),” *Comput. Vis. Image Underst.*, vol. 110, no. 3, pp. 346-359, 2008.
- [39] E. Rublee, V. Rabaud, K. Konolige, and G. Bradski, “ORB: An efficient alternative to SIFT or SURF,” In *Proc. IEEE Int. Conf. Comput. Vis. (ICCV)*, 2011, pp. 2564 -2571.
- [40] S. Leutenegger, M. Chli, and R. Y. Siegwart, “BRISK: Binary Robust invariant scalable keypoints,” In *Proc. IEEE Int. Conf. Comput. Vis. (ICCV)*, 2011, pp. 2548-2555.
- [41] P. F. Alcantarilla, A. Bartoli, and A. J. Davison, “Kaze features,” In *Proc. Eur. Conf. Comput. Vis. (ECCV)*, 2012, pp. 214-227.
- [42] P. F. Alcantarilla, J. Nuevo, and A. Bartoli, “Fast explicit diffusion for accelerated features in nonlinear scale spaces,” In *Proc. Brit. Mach. Vis. Conf. (BMVC)*, 2013.
- [43] E. Simo-Serra *et al.*, “Discriminative learning of deep convolutional feature point descriptors,” In *Proc. IEEE Int. Conf. Comput. Vis. (ICCV)*, 2015, pp. 118 -126.
- [44] V. Balntas, E. Riba, D. Ponsa, and K. Mikolajczyk, “Learning local feature descriptors with triplets and shallow convolutional neural networks,” In *Proc. Brit. Mach. Vis. Conf. (BMVC)*, 2016, pp. 119.1-119.11.
- [45] V. Balntas, E. Johns, L. Tang, and K. Mikolajczyk, “PN-Net: Conjoined Triple Deep Network for Learning Local Image Descriptors,” *arXiv preprint arXiv:1601.05030*, 2016.
- [46] B. G. Vijay Kumar, G. Carneiro, and I. Reid, “Learning Local Image Descriptors with Deep Siamese and Triplet Convolutional Networks by Minimizing Global Loss Functions,” In *Proc. IEEE Conf. Comput. Vis. Pattern Recognit. (CVPR)*, 2016, pp. 5385-5394.
- [47] X. Zhang, F. X. Yu, S. Kumar and S. Chang. “Learning Spread-Out Local Feature Descriptors,” In *Proc. IEEE Int. Conf. Comput. Vis. (ICCV)*, 2017, pp. 4605-4613.
- [48] T. Yang, J. Hsu, Y. Lin, and Y. Chuang, “DeepCD: Learning Deep Complementary Descriptors for Patch Representations,” In *Proc. IEEE Int. Conf. Comput. Vis. (ICCV)*, 2017, pp. 3334-3342.
- [49] S. Wang *et al.*, “Better and Faster: Exponential Loss for Image Patch Matching,” In *Proc. IEEE Int. Conf. Comput. Vis. (ICCV)*, 2019, pp. 4811-4820.
- [50] Y. Tian *et al.*, “SOSNet: Second order similarity regularization for local descriptor learning,” In *Proc. IEEE Conf. Comput. Vis. Pattern Recognit. (CVPR)*, 2019, pp. 11008-11017.
- [51] Y. Tian, A. Barroso-Laguna, T. Ng, V. Balntas, and K. Mikolajczyk, “HyNet: Learning local descriptor with hybrid similarity measure and triplet loss,” In *Proc. Adv. Neural Inf. Process. Syst. (NeurIPS)*, 2020, pp. 1-12.
- [52] Y. Tian, B. Fan, and F. Wu, “L2-Net: Deep learning of discriminative patch descriptor in Euclidean space,” In *Proc. IEEE Conf. Comput. Vis. Pattern Recognit. (CVPR)*, 2017, pp. 661 -669.
- [53] A. Mishchuk, D. Mishkin, F. Radenović, and J. Matas, “Working hard to know your neighbor’s margins: Local descriptor learning loss,” In *Proc. Adv. Neural Inf. Process. Syst. (NeurIPS)*, 2017, pp. 4827-4838.
- [54] C. Wang, X. Lan, and X. Zhang, “How to train triplet networks with 100K identities,” In *Proc. IEEE Int. Conf. Comput. Vis. Workshops (ICCVW)*, 2017, pp. 1907-1915.
- [55] W. Zheng, Z. Chen, J. Lu, and J. Zhou, “Hardness-aware deep metric learning,” In *Proc. IEEE Conf. Comput. Vis. Pattern Recognit. (CVPR)*, 2019, pp. 72-81.
- [56] X. Han, T. Leung, Y. Jia, R. Sukthankar, and A. C. Berg, “MatchNet: Unifying feature and metric learning for patch-based matching,” In *Proc. IEEE Conf. Comput. Vis. Pattern Recognit. (CVPR)*, 2015, pp. 3279-3286.
- [57] S. Zagoruyko and N. Komodakis, “Learning to compare image patches via convolutional neural networks,” In *Proc. IEEE Conf. Comput. Vis. Pattern Recognit. (CVPR)*, 2015, pp. 4353-4361.
- [58] M. Hassanin, S. Anwar, I. Radwan, F. S. Khan, and A. Mian, “Visual attention methods in deep learning: An in-depth survey,” *arXiv preprint arXiv:2204.07756*, 2022.
- [59] A. Vaswani *et al.*, “Attention is all you need,” In *Proc. Adv. Neural Inf. Process. Syst. (NeurIPS)*, 2017.
- [60] X. Wang, R. Girshick, A. Gupta, and K. He, “Non-local Neural Networks,” In *Proc. IEEE Conf. Comput. Vis. Pattern Recognit. (CVPR)*, 2018, pp. 7794-7803.
- [61] H. Zhang, I. Goodfellow, D. Metaxas, and A. Odena, “Self-attention generative adversarial networks,” In *Proc. Int. Conf. Mach. Learn. (ICML)*, 2019, pp. 12744-12753.
- [62] J. Hu, L. Shen, S. Albanie, G. Sun, and E. Wu, “Squeeze-and-excitation networks,” *IEEE Trans. Pattern Anal. Mach. Intell.*, vol. 42, no.8, pp. 2011-2023, 2020.
- [63] Q. Wang *et al.*, “ECA-Net: Efficient Channel Attention for Deep Convolutional Neural Networks,” In *Proc. IEEE Conf. Comput. Vis. Pattern Recognit. (CVPR)*, 2020, pp. 11531-11539.
- [64] H. Zhang *et al.*, “ResNeSt: Split-Attention Networks,” In *Proc. IEEE Conf. Comput. Vis. Pattern Recognit. Workshops (CVPRW)*, 2022, pp. 2735-2745.
- [65] M. Jaderberg, K. Simonyan, A. Zisserman, and K. Kavukcuoglu, “Spatial transformer networks,” In *Proc. Adv. Neural Inf. Process. Syst. (NeurIPS)*, 2015, pp. 2017-2025.
- [66] S. Woo, J. Park, J. Lee, and I. Kweon, “CBAM: Convolutional Block Attention Module,” In *Proc. Eur. Conf. Comput. Vis. (ECCV)*, 2018, pp. 3-19.
- [67] T. Zhao and X. Wu, “Pyramid feature attention network for saliency detection,” In *Proc. IEEE Conf. Comput. Vis. Pattern Recognit. (CVPR)*, 2019, pp. 3080-3089.
- [68] C. Li *et al.*, “Spatial attention pyramid network for unsupervised domain adaptation,” In *Proc. Eur. Conf. Comput. Vis. (ECCV)*, 2020, pp. 481-497.
- [69] Z. Huang *et al.*, “CCNet: Criss-cross attention for semantic segmentation,” *IEEE Trans. Pattern Anal. Mach. Intell.*, vol.45, no.6, pp. 6896-6908, 2023.
- [70] Y. Cao, J. Xu, S. Lin, F. Wei, and H. Hu, “GCNet: Non-Local Networks Meet Squeeze-Excitation Networks and Beyond,” In *Proc. IEEE Int. Conf. Comput. Vis. Workshops (ICCVW)*, 2019, pp. 1971-1980.
- [71] J. Fu *et al.*, “Dual Attention Network for Scene Segmentation,” In *Proc. IEEE Conf. Comput. Vis. Pattern Recognit. (CVPR)*, 2019, pp. 3141-3149.
- [72] J. Johnson, A. Alahi, and F. Li, “Perceptual losses for real-time style transfer and super-resolution,” In *Proc. Eur. Conf. Comput. Vis. (ECCV)*, 2016, pp. 694-711.
- [73] K. Simonyan and A. Zisserman, “Very deep convolutional networks for large-scale image recognition,” In *Proc. Int. Conf. Learn. Represent. (ICLR)*, 2015.
- [74] J. Deng *et al.*, “ImageNet: A Large-Scale Hierarchical Image Database,” In *Proc. IEEE Conf. Comput. Vis. Pattern Recognit. (CVPR)*, 2009, pp. 248-255.
- [75] M. Brown and S. Süssstrunk, “Multi-spectral SIFT for scene category recognition,” In *Proc. IEEE Conf. Comput. Vis. Pattern Recognit. (CVPR)*, 2011, pp. 177-184.
- [76] Y. Xiang, R. Tao, F. Wang, H. You, and B. Han, “Automatic registration of optical and SAR images via improved phase congruency model,” *IEEE J. Sel. Top. Appl. Earth Observ. Remote Sens.*, vol. 13, pp. 5847-5861, 2020.
- [77] M. Schmitt, L. H. Hughes, C. Qiu, and X. Zhu, “SEN12MS—A curated dataset of georeferenced multi-spectral sentinel-1/2 imagery for deep learning and data fusion,” *ISPRS Ann. Photogramm. Remote Sens. Spatial Inf. Sci.*, vol. 40, no. 2, pp. 153-160, 2019.
- [78] M. A. Fischler and R. C. Bolles, “Random sample consensus: A paradigm for model fitting with applications to image analysis and automated cartography,” *Commun. ACM*, pp. 381-395, 1981.